

N-Doping Induced Lattice Expansion of 1D Template Confined Ultrathin MoS₂ Sheets to Significantly Enhance Lithium Polysulfides Redox Kinetics for Li–S Battery

Minzhe Chen, Nan Wang, Wei Zhou, Xiaoyan Zhu, Qikai Wu, Ming-Hsien Lee, Dengke Zhao,* Shunlian Ning,* Maozhong An,* and Ligui Li*

Preparing MoS₂-based materials with reasonable structure and catalytic activity to enhance the sluggish kinetics of lithium polysulfides (LiPSs) conversion is of great significance for Li-S batteries (LSBs) but still remain a challenge. Hence, hollow nanotubes composed of N-doped ultrathin MoS₂ nanosheets (N-MoS₂ NHTs) are fabricated as efficient S hosts for LSBs by using CdS nanorods as a sacrifice template. Characterization and theoretical results show that the template effectively inhibits the excessive growth of MoS₂ sheets, and N doping expands the interlayer spacing and modulates the electronic structure, thus accelerating the mass/electron transfer and enhancing the LiPSs adsorption and transformation. Benefiting from the merits, the N-MoS2 NHTs@S cathode exhibits an excellent initial capacity of 887.8 mAh g⁻¹ and stable cycling performances with capacity fading of only 0.0436% per cycle at 1.0 C (500 cycles). Moreover, even at high S loading that of 7.5 mg cm⁻², the N-MoS₂ NHTs@S cathode also presents initial excellent areal capacity of 7.80 mAh cm⁻² at 0.2 C. This study offers feasible guidance for designing advanced MoS₂-based cathode materials in LSBs.

1. Introduction

Lithium-sulfur batteries (LSBs) owing to inexpensive cost, extraordinary theoretical capacity (1675 mAh g⁻¹) and energy density (2600 Wh kg⁻¹) are considered to be one of the most favorable energy storage solutions to meet the current energy crisis.[1,2] Unfortunately, despite years of research, many inherent factors of sulfur cathode, such as insulating nature of sulfur and discharge products (Li₂S/Li₂S₂), severe volume expansion (next to 80%), and the "shuttle effect" remain unsolved, thus resulting in low sulfur utilization, poor rate performance, and cycle life, which severely restrict the largescale application of LSBs.[3-5] To deal with the problems, numerous efforts have been devoted to design advanced sulfur hosting cathode such like porous carbon,[6] metal oxides,[7] sulfides,[8] and nitrides.[9] Among

M. Chen, W. Zhou, X. Zhu, Q. Wu, L. Li New Energy Research Institute School of Environment and Energy South China University of Technology Higher Education Mega Center 382 East Waihuan Road, Guangzhou 510006, China E-mail: esguili@scut.edu.cn

N. Wang
Siyuan Laboratory
Guangzhou Key Laboratory of Vacuum Coating Technologies and New
Energy Materials
Department of Physics
Jinan University
Guangzhou, Guangdong 5 10632, China
M.-H. Lee
Department of Physics
Tamkang University
New Taipei 25137, Taiwan

Henan Normal University Xinxiang 453007, China E-mail: zhaodengke@htu.edu.cn S. Ning School of Chemistry Sun Yat-sen University Guangzhou, Guangdong 5 10275, China E-mail: ningshlian@mail2.sysu.edu.cn MIIT Key Laboratory of Critical Materials Technology for New Energy Conversion and Storage School of Chemistry and Chemical Engineering Harbin Institute of Technology Harbin, Heilongjiang 150001, China E-mail: mzan@hit.edu.cn State Key Laboratory of Urban Water Resource and Environment School of Chemistry and Chemical Engineering

The ORCID identification number(s) for the author(s) of this article can be found under https://doi.org/10.1002/smll.202303015

DOI: 10.1002/smll.202303015

D. Zhao

School of Materials Science and Engineering

Harbin Institute of Technology Harbin 150001, China

16136829, 2023, 48, Downoladed from https://onlinelbray.wiley.com/doi/10.1002/smll.20230315 by National Taiwan University, Wiley Online Library on [05/12/2023], See the Terms and Conditions (https://onlinelibray.wiley.com/terms-and-conditions) on Wiley Online Library for rules of use; OA articles are governed by the applicable Creative Commons Licenses

www.small-journal.com

them, MoS_2 has been got widespread concern due to the unique S–Mo–S like sandwich structure and good adsorption and catalytic capacity of lithium polysulfides (LiPSs). [10,11] However, severe stacking between lamellae can be occurred in conventional MoS_2 due to the van der Waals forces, which is not conducive to high sulfur leading and fully expose the active sites. [12,13] Those disadvantages make MoS_2 -based materials not satisfy the complex cathodic sulfur conversion reaction in LSBs.

The morphology and electronic structure of materials greatly affect their performance in LSBs. For examples, a large number of researches (Ni-Fe-P/NC,[14] NiS2CPCF,[15] and CNTs/Co₃S₄@NC^[16]) have proven that the hollow architectures can provide more sulfur storage spaces, expose more electrodeelectrolyte contact areas, and alleviate volume changes during cycling compared to other structures, thus exhibits higher battery performance and stability. Moreover, many theoretical and experimental results shown that reasonably regulating electronic structure by doping suitable heteroatoms can enhance the kinetic and reduce the energy barriers in battery reaction, which can also significantly enhance the performance of the battery. For instance, the Co_{0.9}Zn_{0.1}Te₂@NC shows much more enhanced battery performance than CoTe₂@NC because the lattice strain induced by Zn doping changes the coordination environment and electronic mechanism around Co to balance the adsorption and catalysis of LiPSs.[17] Inspired by the above, assembling MoS2 nanosheets into hierarchical hollow architectures and further regulating its electronic structure by heteroatom doping is a feasible strategy to solve the issues of MoS2 and realize their full merits in LSBs.[18-20] However, based on the strong van der Waals forces on MoS₂ layers, how to simultaneously control the MoS₂based materials with highly uniform hollow architectures and appropriate electronic structure by a simple way is still a significant challenge.

Herein, we develop 1D highly uniform hollow nanotube composed of N-doped ultrathin MoS2 nanosheets (N-MoS2 NHTs) as versatile cathode materials for LSBs batteries by a simple hydrothermal-nitridation route using CdS nanorods (CdS NRs) as the sacrificial templates. Characterization and theoretical results show that unique 1D hollow architectures increase the S loading. In addition, N doping modulates the electrons in MoS₂ and induces layer spacing expansion, which is accelerating the mass/electron transfer and enhancing the chemisorption and transforming ability of LiPSs. In consequence, N-MoS₂ NHTs@S cathode presents significant advancements in the operation of LSBs, which exhibits excellent initial capacity (1276.9, 887.8, and 733.7 mAh g^{-1} at 0.1, 1.0, and 2.0 C, respectively) and relative low polarization. Moreover, even in high sulfur loading mass (7.5 mg cm⁻²), it also presents brilliant initial areal capacity of 7.80 mAh cm⁻² and the capacity keeps alive in 4.80 mAh cm⁻² with better capacity-retention (CR) of 61.54% after 100 cycles.

2. Result and Discussion

Figure 1a illustrates the synthesis details of N-MoS₂ NHTs@S sample. At first, the uniform and smooth CdS NRs with a diameter of ≈100 nm are obtained via one-step hydrothermal reaction (Figure S1a, Supporting Information). Subsequently, the well-uniform MoS₂ nanosheets are uniformly wrapped on the

smooth surface of CdS NRs (MoS2@CdS NRs) via the hydrothermal reaction, which still maintain the nanorod structure with a roughened surface appearance (Figure S1b, Supporting Information). Then, the N-MoS₂ NHTs are obtained by annealing. Because of the CdS templates, N-MoS, NHTs also exhibit the nanorod-like morphology (Figure S1c, Supporting Information). The main compared sample (MoS₂ NHTs) indicates the similar morphology with N-MoS₂ NHTs (Figure S1e, Supporting Information). By contrast, the MoS₂ without CdS templates presenting the flowers-like morphology is calcined under the same pyrolysis process (Figure S1d, Supporting Information). The results show that the CdS templates can effectively control the morphology of MoS₂. Finally, the S powders are combined with the as-prepared materials through conventional melt diffusion method to form N-MoS₂ NHTs@S. In Figure S1f of the Supporting Information, the N-MoS2 NHTs@S can still retain their former nanorod morphology, and no apparent large sulfur particles can be found, demonstrating the most of S powders are confined to the hollow tube.

Furthermore, the TEM is further carried out to evaluate the unique interlayer structure of N-MoS $_2$ NHTs sample. Figure 1b indicates that N-MoS $_2$ NHTs shows a hollow tube structure with diameters of $\approx\!80$ nm. In addition, in Figure 1c, one can find that the number of layers of MoS $_2$ in N-MoS $_2$ NHTs is $\approx\!2-3$ layers, less than that MoS $_2$ without CdS templates ($\approx\!10$ layers) (Figure S2a,b, Supporting Information), suggesting that confinement effect of template inhibits the aggregation of MoS $_2$ nanosheets, thus reducing the number of layers (Figure 1d). As a result, a larger number of active sites are exposed.

The more phase information of as-prepared samples is analyzed by HRTEM images. In Figure 1e, one can find that N-MoS₂ NHTs show obvious lattice spacings of 0.645 nm, belonging to MoS₂ (002) plane. [21] Moreover, selected area electron diffraction (SAED) further confirms above results, the clear diffraction ring attributing to the characteristic (002) facets of MoS2 can be observed in Figure 1e inset. Moreover, in Figure S3 of the Supporting Information, there are many defects can be observed in the N-MoS₂ NHTs due to N doping.^[22] Compared to N-MoS₂ NHTs, by seeing the HRTEM images of MoS2 NHTs, the lattice spacings is only 0.616 nm (Figure S4, Supporting Information), smaller than that of N-MoS₂ NHTs. This may be due to the expansion of MoS₂ layer spacing induced by N doping (Figure 1f). Additionally, the element distribution of N-MoS₂ NHTs is also studied by TEM-mapping. In Figure 1g, one can find that the Mo, S, C, N, O are evenly distributed on the whole hollow structure, and the corresponding element contents are evaluated by EDS-TEM spectra, which are 18.42, 38.43, 25.08, 7.50, and 10.57 at%, respectively. All above results indicate the target materials have been successfully synthesized.

By seeing the XRD pattern (Figure 1h), N-MoS $_2$ NHTs exhibit the six obvious diffraction peaks arising at about $2\theta=14^\circ$, 26° , 33° , 39° , 50° , and 58° , which can be indexed to 2H-MoS $_2$ (PDF#37-1492) and graphite 2H-C (PDF#75-1621), respectively. And, the MoS $_2$ NHTs present similar peak shape of N-MoS $_2$ NHTs, which confirms that crystal phase is not changed after N doping. Interestingly, the main peak is shifted to bigger angle direction compared to N-MoS $_2$ NHTs, which is accordance with the HRTEM results and further confirms that N doping induces the enlargement of MoS $_2$ interlayer spacing. And the intensity

16136829, 2023, 48, Downloaded from https://onlinelibrary.wiley.com/doi/10.1002/sml1.202303015 by National Taiwan University, Wiley Online Library on [05/12/2023]. See the Terms and Conditions (https://onlinelibrary.wiley.com/nerms

) on Wiley Online Library for rules of use; OA articles are governed by the applicable Creative Commons License

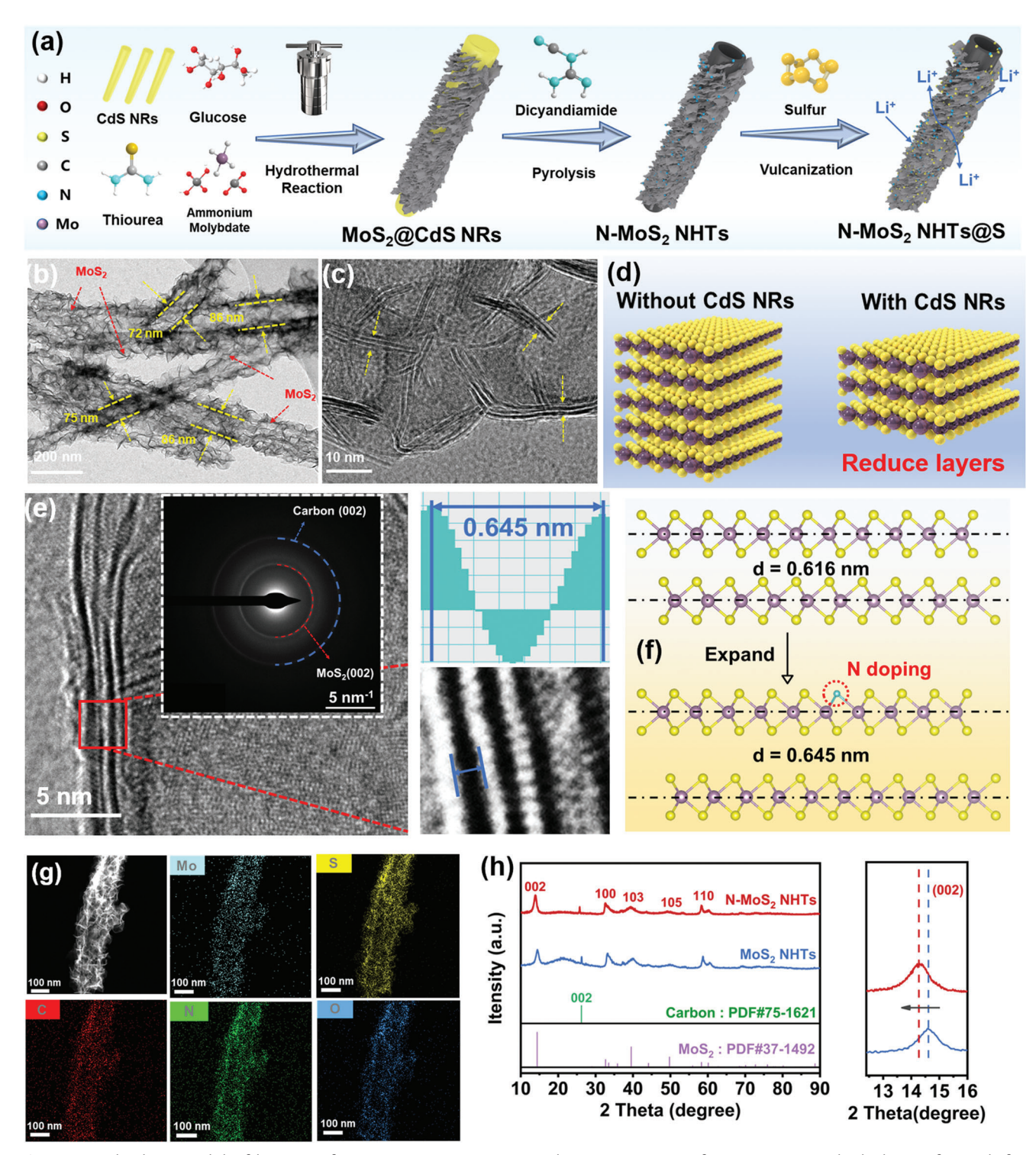


Figure 1. a) The design and the fabrication of N-MoS $_2$ NHTs@S composites. b,c) HRTEM images for N-MoS $_2$ NHTs. d) The layers of MoS $_2$ before using CdS NRs template. e) The HRTEM and FFT plots images for N-MoS₂ NHTs, where the inset is the SAED pattern. f) The change of interlayer space after N doping. g) Element mappings (Mo, S, C, N, O) of N-MoS₂ NHTs. h) XRD patterns of the MoS₂ NHTs and N-MoS₂ NHTs.

www.small-journal.com

16136829, 2023, 48, Downoladed from https://onlinelbray.wiley.com/doi/10.1002/smll.20230315 by National Taiwan University, Wiley Online Library on [05/12/2023], See the Terms and Conditions (https://onlinelibray.wiley.com/terms-and-conditions) on Wiley Online Library for rules of use; OA articles are governed by the applicable Creative Commons Licenses

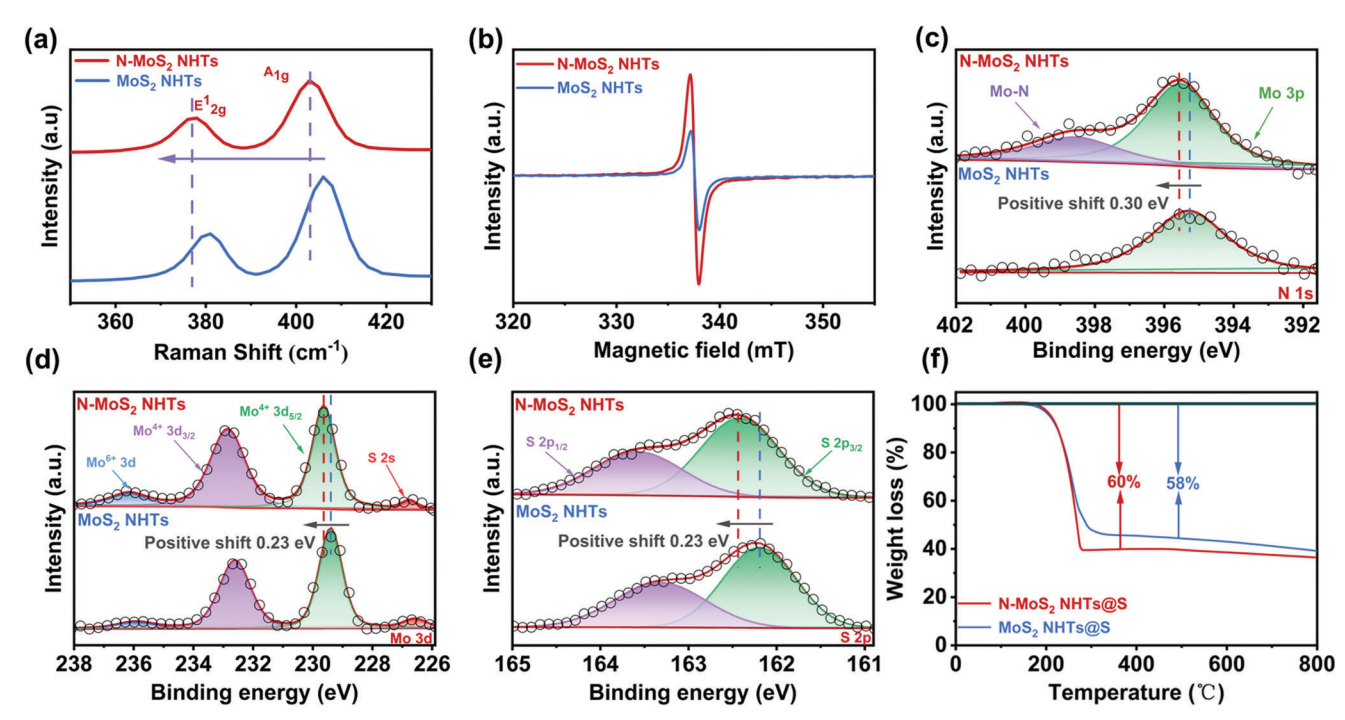


Figure 2. a) Raman spectra and b) EPR patterns of N-MoS₂ NHTs and MoS₂ NHTs. High-resolution XPS spectra of c) N 1s, d) Mo 3d, and e) S 2p regions of N-MoS₂ NHTs and MoS₂ NHTs. f) TGA of N-MoS₂ NHTs@S and MoS₂ NHTs@S under N₂ atmosphere.

of N-MoS $_2$ NHTs is lower than that of MoS $_2$ NHTs indicating the smaller MoS $_2$ layers of N-MoS $_2$ NHTs (Figure S5, Supporting Information), which correspond to the result of HRTEM. Raman spectra (**Figure 2a**) of samples exhibit two characteristic peaks at 378 and 403 cm $^{-1}$, which correspond to the $E_{2g}^{\ 1}$ and A_{1g} of MoS $_2$, respectively. The $E_{2g}^{\ 1}$ involves in-layer displacements of Mo and S atoms, and the A_{1g} stands for out-of-layer symmetric displacements of S atoms along the c-axis. [23,24] Most importantly, the peaks of them both shift negatively after N doping, which is also strong evidence to testify the expansion of interlayer space. In EPR spectra (Figure 2b), where the g-value of 2.002 can be assigned to S vacancy sites from excess unpaired electrons in MoS $_2$, and the N-MoS $_2$ NHTs show the higher peak density than MoS $_2$ NHTs, further indicating that there are more defects in N-MoS $_2$ NHTs after N doping.

Then, to investigate the valence state and chemical composition, the XPS analysis is performed. In high-resolution N1s spectra (Figure 2c), N-MoS2 NHTs exhibit two peaks after deconvolution, ascribing to Mo-N peak (398.57 eV) and Mo 3p peak (395.53 eV), respectively.[25,26] The appearance of Mo-N bond after N doping further confirms that the N atoms successfully doped in to MoS2. Moreover, one can find that the bind energy (BE) of Mo 3p positively shifts ≈0.3 eV compared to MoS₂ NHTs, which suggest that the N doping can effectively regulate the electronic structure of MoS₂. The Mo 3d spectra further prove the results. In Figure 2d, two fairly high peaks can be observed in Mo3d spectra of N-MoS₂ NHTs, which are belonging to Mo⁴⁺ (232.85/229.63 eV) and Mo⁶⁺ (236.16 eV).^[27] Furthermore, the BE of Mo 3d shows a clearly positive shift compared to that of MoS₂ NHTs sample. The S 2p spectra of N-MoS2 NHTs (Figure 2e) present two peaks (S $2p_{1/2}$ in 163.57 eV and S $2p_{3/2}$ in 162.42 eV for S—S bonding of MoS₂),^[28] which further prove the existence of 2H

MoS₂. And the positive shift of BE of S 2p also demonstrates the effective adjustment of electronic structure by N doping, which can help to improve the catalytic and adsorption capacity toward LiPSs.^[29]

To investigate the properties of N-MoS₂ NHTs in LSBs, the relevant S cathode composites, named N-MoS2 NHTs@S, are fabricated (see the Experiments Section for details). In Figure S6 of the Supporting Information, N-MoS2 NHTs@S show the distinct diffraction peaks being consistent with sulfur (PDF#89-2600), suggesting that the successful immersion of sulfur into the host materials. The specific surface area (SSA) and average pore volume (APV) of the materials also play important roles for performance in LSBs,^[30] which can be analyzed by the N₂ adsorptiondesorption measurements. In Figure S7a,b of the Supporting Information, the N-MoS₂ NHTs possess the appropriate SSA $(52.420 \text{ m}^2 \text{ g}^{-1})$ and APV $(0.220 \text{ cm}^3 \text{ g}^{-1})$, which suggest that N-MoS₂ NHTs can provide much S storage. After S loading (Figure S7c, Supporting Information), the SSA and APV reduce to 12.075 m² g⁻¹ and 0.045 cm³ g⁻¹, respectively, indicating S has been infiltrated into pore and channels. In addition, the load capacity of S is estimated via TGA (Figure 2f), which are \approx 60% and 58% for N-MoS2 NHTs@S and MoS2 NHTs@S, respectively, which further prove that the N-MoS₂ NHTs have a high S storage capacity.

In order to analyze the anchoring ability of as-prepared samples toward LiPSs, visual adsorption measurements (VAM) are carried out. In **Figure 3**a inset, one can find that the N-MoS₂ NHTs/Li₂S₆ solution has been changed from brown-yellow to almost clarified after 1.0 h compared to MoS₂ NHTs/Li₂S₆ solution, demonstrating that N doping can boost the adsorption LiPSs ability. Additionally, these corresponding UV–vis spectra (Figure 3a) between the range of 200–800 nm confirmed the results, in which N-MoS₂ NHTs/Li₂S₆ shows the lowest Li₂S₆-relevant absorbance

16136829, 2023, 48, Downloaded from https://onlinelibrary.wiley.com/doi/10.1002/smll.202303015 by National Taiwan University, Wiley Online Library on [05/12/2023]. See the Terms and Conditions (https://onlinelibrary.wiley.com/terms-

onditions) on Wiley Online Library for rules of use; OA articles are governed by the applicable Creative Commons License

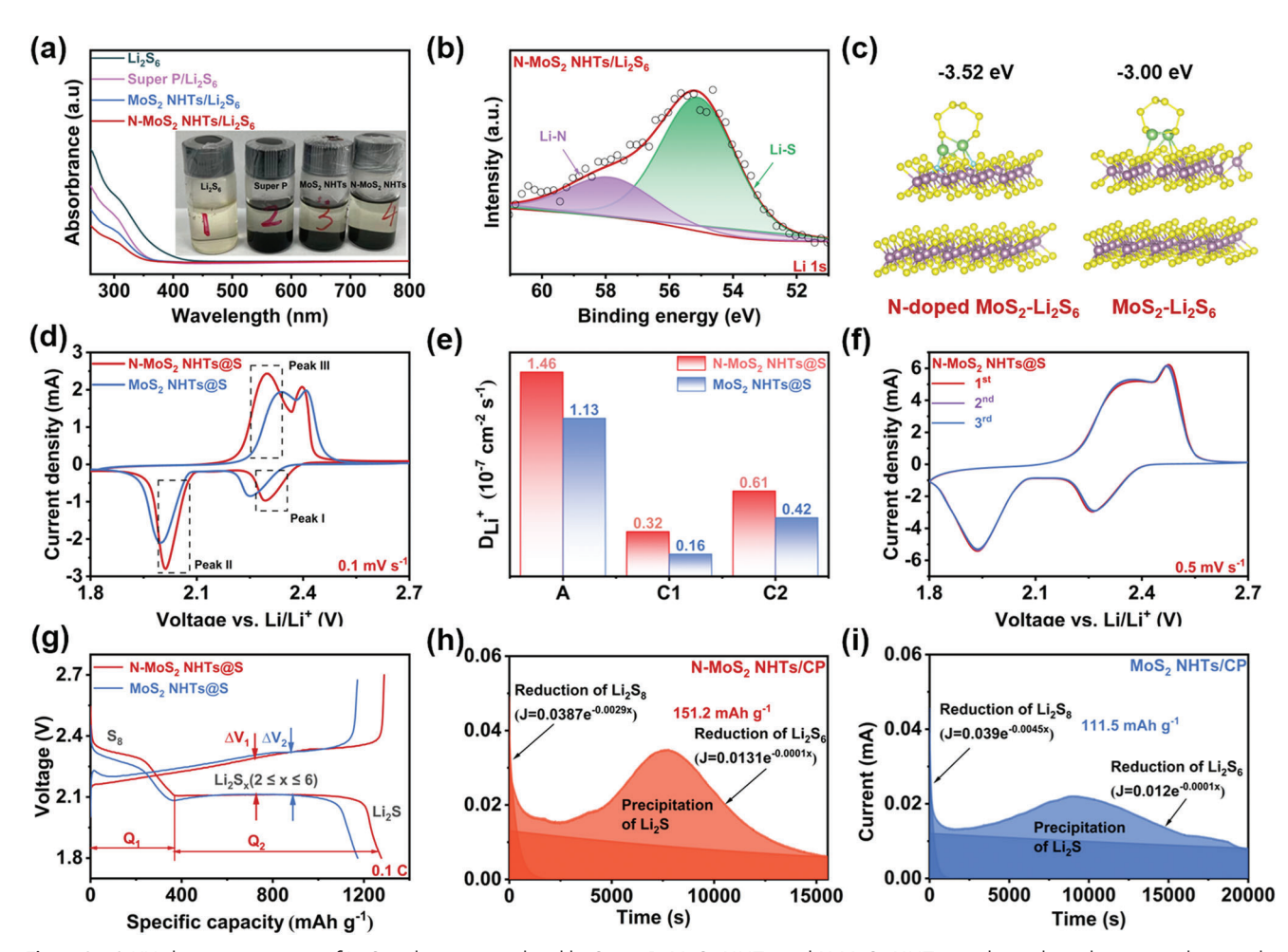


Figure 3. a) UV absorption spectra of Li_2S_6 solution assimilated by Super P, MoS_2 NHTs, and N-MoS $_2$ NHTs powders, where the inset is the straightforward phenomenon of the Li_2S_6 adsorption experiments. b) XPS of Li1s regions of N-MoS $_2$ NHTs after soaking in Li_2S_6 . c) The optimal adsorption configuration of Li_2S_6 on MoS $_2$ and N-doped MoS $_2$. d) CV curves at 0.1 mV s $^{-1}$ and e) the Li $^+$ diffusion coefficient. f) Three cycles of CV curves of N-MoS $_2$ NHTs cathode at 0.5 mV s $^{-1}$. g) The galvanostatic charge and discharge (GCD) at 0.1 C curves. Li_2S deposition profiles of h) N-MoS $_2$ NHTs/CP and i) MoS $_2$ NHTs/CP.

peaks. To deeply reveal the high-adsorption capacity of LiPSs, the MoS₂ NHTs and N-MoS₂ NHTs after VAM are also characterized by XPS. In XPS spectrum (Figure S8a, Supporting Information), where one can find a new formed peak (Li 1s), which indicates that the LiPSs are adsorbed on the sample. Additionally, from high-resolution Li1s spectrum (Figure 3b), two fitting peaks attributed to Li-S (56.63 eV) and Li-N (58.43 eV) can be observed, the formation of Li-N bond confirms that N doping enhances the lithiophilic property of MoS₂, thus boosting the adsorption capacity of LiPSs. [31,32] Furthermore, theoretical calculation also proves the Li₂S₆ can be easier to adsorb on N-MoS₂ NHTs. In Figure 3c, one can find that the Li₂S₆ can be adsorbed on N sites and S sites after N doping, thus N-doped MoS, show lower adsorption energy (-3.52 eV) than that of MoS₂ (-3.00 eV). The N 1s, Mo 3d, and S 2p spectra (Figure S8b-d, Supporting Information) also demonstrate that there is strong chemisorption between Li₂S₆ and N-MoS2 NHTs, the BE of N 1s and Mo 3d are shifted after VAM. Moreover, it is remarkable that the double peaks discovered in 169.74 and 168.32 eV signify polysulfate and thiosulfate, which are both the intermediate of LiPSs conversion.[33] The formation

of intermediate indicates that N-MoS $_2$ NHTs display rapid redox kinetics of LiPSs conversion. In addition, by seeing the XPS spectra of MoS $_2$ NHTs after adsorption experiment (Figure S9, Supporting Information), no obvious Li—N bonds can be observed, which further indicate that N doping can enhance the adsorption capacity toward LiPSs by the strong chemical interaction, and therefore more effective suppression of the "shuttle effect" to improve the cycling stability and utilization of S for LSBs.

Then, the electroactivity of the N-MoS₂ NHTs@S cathode (S load ≈ 1.2 mg cm⁻²) is assembled by systematic electrochemical testing. In Figure 3d, CV curves shows two significant cathodic peaks at ≈ 2.3 and 2.0 V, ascribing to the reduction conversion of S₈ to the high-order LiPSs (Li₂S_x, $4 \le x \le 8$) and next change to low-order insoluble Li₂S/Li₂S₂, and two evident anodic peaks at ≈ 2.3 and 2.4 V are attributed to the transition of Li₂S/Li₂S₂ to long-chain Li₂S_x and S₈.^[34] The voltage gap (ΔV) between reduction and oxidation peaks of N-MoS₂ NHTs@S cathode is only 388 mV, lower than that of MoS₂ NHTs@S ($\Delta V = 412$ mV). Moreover, N-MoS₂ NHTs@S has the higher current peaks (I_p) both in oxidation and reduction process compared to MoS₂

16136829, 2023, 48, Downoladed from https://onlinelbray.wiley.com/doi/10.1002/smll.20230315 by National Taiwan University, Wiley Online Library on [05/12/2023], See the Terms and Conditions (https://onlinelibray.wiley.com/terms-and-conditions) on Wiley Online Library for rules of use; OA articles are governed by the applicable Creative Commons Licenses

www.small-journal.com

NHTs@S, which shows that N-MoS₂ NHTs@S exhibits faster redox kinetics with low polarization during the cell reaction. Tafel pots calculated from the CV curves can be used to investigate the electrocatalytic ability.^[35] In Figure S10a–c of the Supporting Information, N-MoS₂ NHTs@S shows lower Tafel slopes that of 66.13, 88.41, and 72.14 mV dec⁻¹ at peak I, peak II, and peak III, respectively, than that of MoS₂ NHTs@S (88.19, 102.8, and 94.78 mV dec⁻¹), further indicating that N-MoS₂ NHTs@S possesses the more excellent redox kinetics for sulfur bidirectional reaction.

In order to deeply understand of the Li⁺ dynamics, the CV tests at different scan rates (0.1–0.5 mV $\rm s^{-1}$) are evaluated (Figure S11a,b, Supporting Information). As the scan rate grows, the anodic and cathodic peaks shift positively and negatively, respectively. The shift values of A, C₁, and C₂ peaks in N-MoS₂ NHTs@S are 75, 34, and 79 mV, respectively, lower than those of MoS₂ NHTs@S (103, 35, and 121 mV), which is the significant signal of the enhanced Li+ diffusivity and reaction kinetics. As depicted in Figure S12a-c of the Supporting Information, the redox peak currents of N-MoS2 NHTs@S and MoS2 NHTs@S being linear with the square root of scanning rates and the slope of the curve is in direct proportion to Li⁺ diffusion rate.^[36] It is distinct that the slopes of N-MoS₂ NHTs@S electrode at three peaks are larger than that of the MoS2 NHTs@S. The Randles-Sevcik equation (detail in the Supporting Information) is used to calculate the Li⁺ diffusion coefficient (D_{Li}^+). Through the analysis, the D_{Li}^+ of N-MoS₂ NHTs@S (A, C₁, C₂: 1.46 × 10⁻⁷, 0.32 × 10⁻⁷, $0.61 \times 10^{-7} \ \mathrm{cm^2 \ s^{-1}})$ are all higher than that of MoS $_2$ NHTs@S (A, C_1 , C_2 : 1.13×10^{-7} , 0.16×10^{-7} , 0.42×10^{-7} cm² s⁻¹) (Figure 3e). Above discussed findings demonstrate that MoS2 NHTs@S significantly enhances the rate of both solid-liquid and liquid-solid

In Figure 3f, the N-MoS₂ NHTs@S cathode can maintain good overlap after three CV cycles at 0.5 mV $\rm s^{-1}$, which demonstrates that N-MoS2 NHTs@S dynamically relieves the dissolution of LiPSs and boosts the its conversion reversibility during discharge/charge process. Figure 3g indicates the galvanostatic charge/discharge (GCD) profiles of N-MoS₂ NHTs@S and MoS₂ NHTs@S at 0.1 C. There are two platforms in discharge curves, in which the first platform belongs to S_8 to Li_2S_n ($4 \le n \le 8$) and the second one is accordance with long chain LiPSs to Li₂S₂/Li₂S.^[37] Especially, the first (1st) and the second (2nd) discharge platform capacity of N-MoS₂ NHTs@S cathode are 373.2 and 915.8 mAh g⁻¹, respectively, both higher than that of the MoS₂ NHTs@S cathode (362.3 and 811.0 mAh g⁻¹). The discharge platform capacity ratio between 2nd and 1st is used to analyze the catalytic efficiency of LiPSs,[38] and the ratio of N-MoS2 NHTs@S cathode is 2.45, better than that of MoS₂ NHTs@S cathode (2.24) (Table S1, Supporting Information). Besides, N-MoS2 NHTs@S cathode also exhibits the smaller polarization value ($\Delta V_1 = 106.6$ mV), further suggesting N-MoS2 NHTs@S possesses exceptional LiPSs mediation capability due to the addition of N atoms to induce interspace expansion of MoS2 and adjust electron distribution.

The electrochemical impedance spectroscopy (EIS) measurement is helpful to estimate as-prepared materials toward sulfur dynamics of conversion. Before cycling, all the samples show one semicircle (high-frequency region) and straight line (low-frequency region), corresponding to charge transfer ($R_{\rm ct}$) and Li⁺ diffusion resistance ($Z_{\rm w}$), respectively (Figure S13a, Supporting

Information). After cycling, additional semicircles both appear in two materials cathodes, which are ascribed to form solid electrode/electrolyte interface [39] (Figure S13c, Supporting Information). Due to electrolyte infiltration, the active substances on the electrode surface are redispersed after cycling. So, the $R_{\rm ct}$ and $Z_{\rm w}$ both become smaller than that of before cycling. By comparison the $R_{\rm ct}$ and $Z_{\rm w}$ of N-MoS $_2$ NHTs@S cathode and MoS $_2$ NHTs@S both before and after cycling (Figure S13b–d, Supporting Information), one can find that the N-MoS $_2$ NHTs@S cathode manifests the much lower $R_{\rm ct}$ (30.575 and 5.353 Ω) and $Z_{\rm w}$ than those of MoS $_2$ NHTs@S (44.185 and 6.028 Ω), which also explain that N doping can greatly enhance the redox kinetics of MoS $_2$ for LiPSs transformation.

Then, the catalytic performances of various materials are further analyzed by symmetric cells test. In corresponding EIS test (Figure S13e, Supporting Information), N-MoS₂ NHTs symmetric cells perform a lower $R_{\rm ct}$ and a steeper slope compared to MoS2 NHTs, suggesting N-MoS2 NHTs are helpful for enhancing the redox kinetics. The CV analyses (Figure S13f, Supporting Information) show that the N-MoS2 NHTs and MoS2 NHTs electrodes both have two pairs of redox peaks, which suggest that there are the redox reactions inside the symmetric cells. In detail, the cathodic peaks A and B belong to reduce S₈ to Li₂S₆ and followingly reduce to Li₂S₂/Li₂S, respectively. The subsequent anodic peaks C and D are corresponding to the inverse oxidation processes.^[40] Compared to MoS₂ NHTs electrode, the N-MoS₂ NHTs electrode shows greater I_p and the smaller ΔV value, which suggests that N-MoS2 NHTs electrode possesses the better electroactivity and kinetics for sulfur bidirectional reaction.

In addition, the Li₂S nucleation experiments are carried out to analyze the catalytic activity of as-prepared samples for LiPSs conversion. In Figure 3h,i, N-MoS₂ NHTs/CP exhibits the higher current value and the precipitation capacity (0.049 mA, 151.2 mAh g⁻¹) than those of MoS₂ NHTs/CP (0.012 mA, 111.5 mAh g⁻¹). A faster conversion rate can generally be inferred from shorter nucleation times. Obviously, the time of nucleation of N-MoS₂ NHTs/CP (9165 s).These results further suggest that N-MoS₂ NHTs enhance electroactivity for conversion of S₈ to the Li₂S_x (4 \leq x \leq 8).

The galvanostatic intermittent titration techniques (GITT) operational test, which can monitor the internal resistance and the lithiation overpotential at various charge-discharge stages, is performed. In Figure S14a,b of the Supporting Information, the two discharge plateaus can be observed, which correspond to the conversion from S₈ to LiPSs, and then following to Li₂S₂/Li₂S. In addition, one charge plateau can also be found, which is attributable to the reaction from Li₂S₂/Li₂S back to S₈. [41] Compared to MoS2 NHTs@S electrode, the N-MoS2 NHTs@S electrode presents higher charge/discharge capacity of 1178.3/1119.9 mAh g⁻¹, Coulombic efficiency of 95.0%, and lower voltage difference (ΔE) of 224 mV between the equilibrium and operating states visualization. Moreover, the resistance curves (Figure S14c,d, Supporting Information) calculated by Equation (S2) of the Supporting Information show that the internal resistances of N-MoS₂ NHTs@S are lower than that of MoS₂ NHTs@S during the charge/discharge procedures, further confirming the N doping can boost the ions transfer and redox kinetics.[42]

Figure 4a shows the rate performance of the prepared materials, revealing that the N-MoS₂ NHTs@S cathode exhibits

16136829, 2023, 48, Downloaded from https://onlinelibrary.wiley.com/doi/10.1002/smll.202303015 by National Taiwan University, Wiley Online Library on [05/12/2023]. See the Terms

on Wiley Online Library for rules of use; OA articles are governed by the applicable Creative Commons

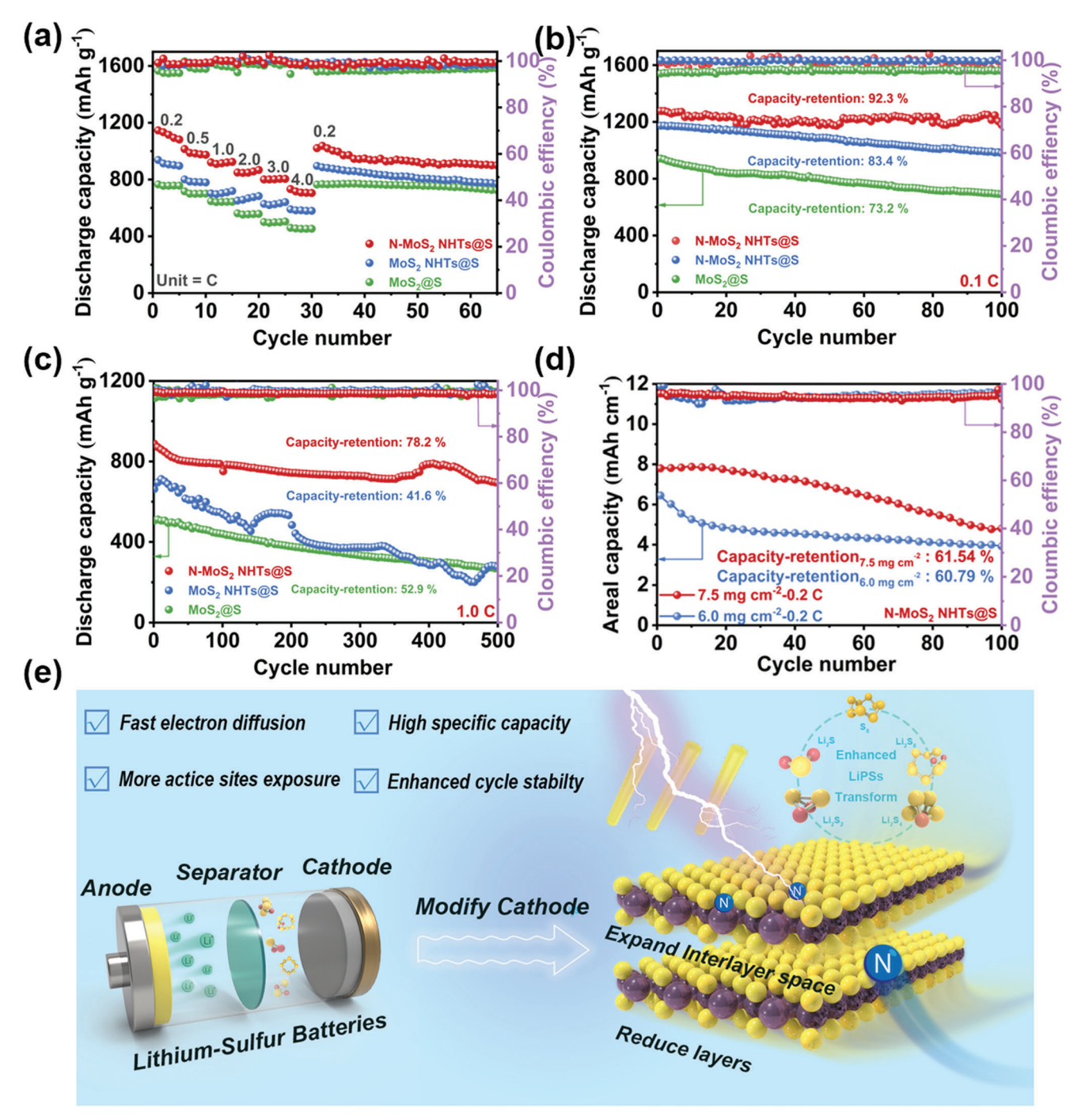


Figure 4. a) Rate (0.2-4 C) performances and persistent behavior at b) 0.1 C and c) 1.0 C of N-MoS₂ NHTs@S, MoS₂ NHTs@S, and MoS₂@S cathodes. d) The areal capacity of N-MoS₂ NHTs@S cathodes under 0.2 C with high sulfur loading. e) Reaction principle of LSBs batteries with N-MoS₂ NHTs@S.

impressive initial discharge capacity (IDC) at different rates (0.2, 0.5, 1.0, 2.0, 3.0, and 4.0 C) of 1145.9, 1014.4, 920.5, 849.2, 800.3, and 732.5 mAh g $^{-1}$, respectively, superior to other comparative samples. The rate switched back to 0.2 C, the N-MoS $_2$ NHTs@S cathode can also maintain the 89.1% capacity (1021.1 mAh g $^{-1}$) of its initial value, which suggests that N-MoS $_2$ NHTs@S possesses the good charge/discharge stability. In addition, by comparing the differences of the corresponding GCD profiles of as-

prepared samples (Figure S15a–c, Supporting Information), one can find that N-MoS₂ NHTs@S shows lower polarization values than those of the comparison samples at different current density (Figure S15d, Supporting Information).

To further study the long-term cycling durability of the N-MoS₂ NHTs@S, the cycling properties at 0.1 C for 100 cycles are first observed in Figure 4b, in which N-MoS₂ NHTs@S shows the high IDC of \approx 1276.9 mAh g⁻¹ and also can maintain high

www.advancedsciencenews.com



16136829, 2023, 48, Downoladed from https://onlinelbray.wiley.com/doi/10.1002/smll.20230315 by National Taiwan University, Wiley Online Library on [05/12/2023], See the Terms and Conditions (https://onlinelibray.wiley.com/terms-and-conditions) on Wiley Online Library for rules of use; OA articles are governed by the applicable Creative Commons Licenses

www.small-journal.com

CR of 92.3% (the 100th cycle capacity is 1178.2 mAh g^{-1}). In comparison, the IDC of MoS₂@S and MoS₂ NHTs@S cathodes are only 941.6 and 1173.1 mAh g⁻¹, much worse than that of N-MoS₂ NHTs@S. Moreover, after cycling test, the CRs are only 83.4% and 73.2%, respectively, further confirming N-MoS₂ NHTs@S has the excellent stability in LSBs. And the specific energy of N-MoS₂ NHTs@S (335.45 Wh kg⁻¹), calculated by Equations (S3) and (S4) of the Supporting Information, is also higher than that of not N-doped materials (308.19 Wh kg⁻¹). The results are also supported by the long-term cycling tests at higher current densities. At 1.0 C, N-MoS2 NHTs@S shows the higher IDC (887.8 mAh g^{-1}) than that of MoS₂@S (506.1 mAh g^{-1}) and MoS₂ NHTs@S (662.6 mAh g⁻¹) cathode (Figure 4c). After 500th cycle, N-MoS2 NHTs@S still keeps the initial capacity of 78.2% (low capacity-decay rate per cycle of 0.0436%), and surpasses the MoS₂@S (52.9%) and MoS₂ NHTs@S (41.6%). Additionally, the N-MoS₂ NHTs@S cathode also can achieve high IDC of 724.7 mAh g⁻¹ with splendid cyclic stability (CR of 61.8% and low capacity-decay rate per cycle of 0.0293%) at 2.0 C (Figure S16, Supporting Information).

LSBs with suitable N/P ratio under high S loading and low electrolyte/sulfur (E/S) ratio ($10 \le \mu L \text{ mg}^{-1}$) condition are necessary for the commercial application. Therefore, the performances of MoS2 NHTs@S and N-MoS2 NHTs@S cathode under high sulfur loading and low E/S are investigated. In Figure 4d, N-MoS₂ NHTs@S with S loading of 6.0 mg cm⁻² exhibits high initial areal capacity of 6.45 mAh cm⁻² at 0.2 C. Remarkably, with a further increase in sulfur loading mass to 7.5 mg cm⁻², N-MoS₂ NHTs@S also deliver high initial areal capacity (7.80 mAh cm⁻²) and CR (61.53%) after 100 cycles. In sharp contrast, MoS₂ NHTs@S cathode under high S loading possesses only low initial areal capacity of 4.74 and 6.45 mAh cm⁻² with CR of 59.11% and 39.81%, respectively (Figure S17, Supporting Information), which suggests that the cyclic stability of MoS2 NHT in high sulfur loading can be enhanced after N doped. The rate performance at high S loading is also investigated (Figure S18a, Supporting Information). Consistent with the low-loading results, the N-MoS2 NHTs@S cathode demonstrates impressive initial areal capacity at various rates (0.2, 0.5, 1.0, and 2.0 C), which are 4.56, 4.14, 3.14, and 2.40 mAh cm⁻², respectively, outperforming other comparative samples. After switching back to 0.2 C, the cathode maintains 98.7% of its initial areal capacity, equivalent to ≈ 4.50 mAh cm⁻² (the average values of 5 cycles). Furthermore, the electrochemical performance of batteries with high sulfur loading is investigated. Even though the ΔV (405 mV) and the R_{ct} (36.485 Ω) all grow due to the increase of the sulfur loading, the batteries with N-MoS₂ NHTs@S still perform better electrochemical performance (Figure S18b,c, Supporting Information). Combined with the above analysis, it can be concluded that as-made N-MoS2 NHTs@S is an excellent S host material for LSBs. As shown in Figure 4e, the outstanding performance of N-MoS₂ NHTs mainly originates from following three reasons. 1) The 1D hollow structure provides more storage space for sulfur, thus increases the S loading.^[43] 2) CdS NR template prevents the aggregation of MoS2 to expose more active sites.[44] 3) The N doping expands the layer space and regulates the electronic structure of MoS2 sheets, which accelerates the mass/electron transfer and enhances the intrinsic activity toward the LiPSs

conversion.

Moreover, DFT calculations are employed to gain insight into the catalytic mechanism of as-prepared samples for S involved reaction. Figure S19 (Supporting Information) and Figure 5a,b show the adsorption model of Li₂S_x on catalyst surface and the corresponding adsorption energy, in which N-doped MoS₂ shows the higher adsorption energy than that of MoS2, indicating Ndoped MoS₂ shows the stronger adsorption capacity toward Li₂S_x. In Figure 5c, the Gibbs free energy change (ΔG) of each step from S₈ to Li₂S is also calculated, where the rate determining step (RDS) is Li₂S₈ converting to Li₂S₆, the N-doped MoS₂ displays the lower ΔG of 0.15 eV, smaller than that of MoS₂ (0.21 eV), suggesting that N doping can effectively decrease the energy barriers of RDS and enhance MoS₂ performance toward the conversion of LiPSs. The density of states (DOS) is beneficial for understanding the inner electronic structure difference, exhibited in Figure 5d,e. Previous studies have shown when the d-band centers are closer to the Fermi level (0 eV), there is a stronger interaction between metal and absorbed LiPSs.^[45] The d-band centers are calculated to be -3.49 eV for MoS₂ and -3.27 eV for N-doped MoS₂, proving that N doping can promote the adsorption of LiPSs. In short, the DFT calculation shows that N doping can lead to the expansion of interlayer space and adjust electron distribution, ultimately enhancing the conversion of LiPSs.

3. Conclusion

In conclusion, we successfully prepare the hollow nanotubes comprised of ultrathin N-doped MoS2 nanosheets as a highly attractive cathode material for LSBs. Combining theoretical calculation with experimental analysis, one can find that N-MoS2 NHTs show high S loading, strong adsorption capacity for LiPSs, and low energy barrier of RDS in cell reaction. Hence, the batteries with N-MoS2 NHTs@S display an excellent performance with the high initial capacity of 1276.9 mAh g⁻¹ at 0.1 C and relatively high CR of 92.3%. Furthermore, even though at 2.0 C, the N-MoS2 NHTs@S cathode can still reach relatively high IDC of 724.7 mAh g⁻¹ and good cyclic stability (low capacity-decay rate per cycle of 0.0293% after 1300 cycles). Under high S loading (7.5 mg cm⁻²), N-MoS₂ NHTs@S still maintains the high initial areal capacity that of 7.80 mAh cm⁻² with good durability (CR of 61.53% after 100 cycles) CR still maintains. This work elucidates a promising path designing advanced MoS2-based cathodes for LSBs through morphology control and doping engineering.

Supporting Information

Supporting Information is available from the Wiley Online Library or from the author.

Acknowledgements

This work was supported by the National Natural Science Foundation of China (52161033 and 22209056), the Fundamental Research Funds for the Central Universities (21620329), the Postdoctoral Research Foundation of China (2020M673071), the Special Funds for the Cultivation of Guangdong College Students' Scientific and Technological Innovation (pdjh2022b0065), the Guangdong Basic and Applied Basic Research Foundation (2023A1515010270), the Science and Technology Planning

16136829, 2023, 48, Downloaded from https://onlinelibrary.wiley.com/doi/10.1002/smll.202303015 by National Taiwan University, Wiley Online Library on [05/12/2023]. See the Terms and Conditions (https://onlinelibrary.wiley.com/doi/10.1002/smll.202303015 by National Taiwan University, Wiley Online Library on [05/12/2023]. See the Terms and Conditions (https://onlinelibrary.wiley.com/doi/10.1002/smll.202303015 by National Taiwan University, Wiley Online Library on [05/12/2023]. See the Terms and Conditions (https://onlinelibrary.wiley.com/doi/10.1002/smll.202303015 by National Taiwan University, Wiley Online Library on [05/12/2023]. See the Terms and Conditions (https://onlinelibrary.wiley.com/doi/10.1002/smll.202303015 by National Taiwan University, Wiley Online Library on [05/12/2023]. See the Terms and Conditions (https://onlinelibrary.wiley.com/doi/10.1002/smll.202303015 by National Taiwan University, Wiley Online Library on [05/12/2023]. See the Terms and Conditions (https://onlinelibrary.wiley.com/doi/10.1002/smll.202303015 by National Taiwan University, Wiley Online Library on [05/12/2023]. See the Terms and Conditions (https://onlinelibrary.wiley.com/doi/10.1002/smll.202303015 by National Taiwan University, Wiley Online Library on [05/12/2023]. See the Terms and Conditions (https://onlinelibrary.wiley.com/doi/10.1002/smll.202303015 by National Taiwan University (https://onlinelibrary.wile

ditions) on Wiley Online Library for rules of use; OA articles are governed by the applicable Creative Commons

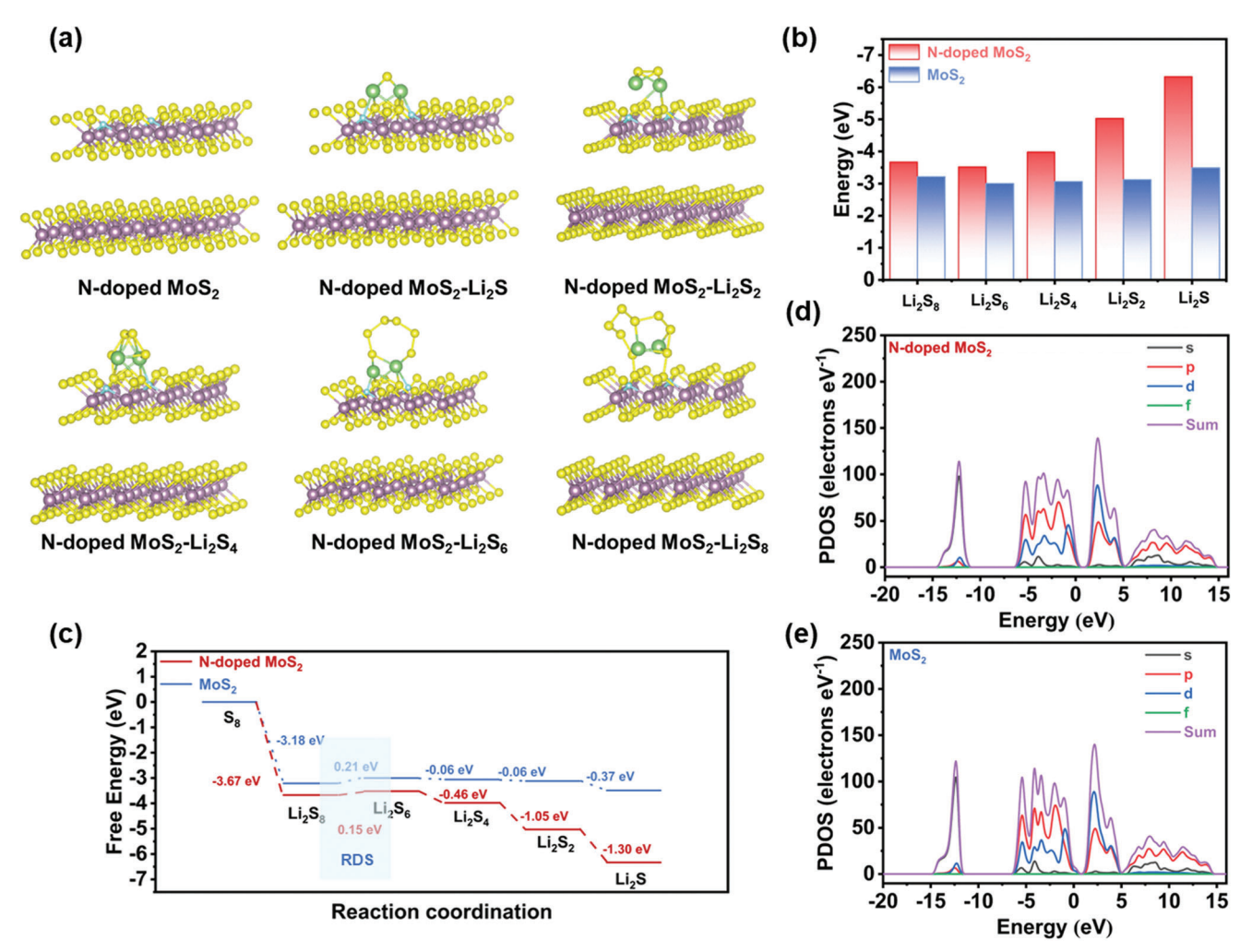


Figure 5. a) The optimal adsorption configuration of Li_2S_x (x = 1, 2, 4, 6, 8) on N-doped MoS₂. b) Adsorption energies of different Li_2S_x (x = 1, 2, 4, 6, 8) materials and c) the calculated free energy of the S reduction on the catalyst. PDOS for d) N-doped MoS₂ and e) MoS₂.

Project of Guangzhou (201605030008 AND 202201010125), the National Innovation and Entrepreneurship Training Program for Undergraduate (202110559044), and the Open Project of State Key Laboratory of Urban Water Resource and Environment, Harbin Institute of Technology (No. QA202133). The authors would like to thank the shiyanjia lab (www.shiyanjia.com) for the xps test.

Conflict of Interest

The authors declare no conflict of interest.

Author Contributions

M.C. and N.W. contributed equally to this work. M.C.: experiment, data curation, analysis, and writing the original draft. W.Z., X.Z., and Q.W.: validation and experimental instruction. S.N.: theoretical calculation. M.-H.L.: theoretical calculation, software. D.Z.: validation, article revision, review, and editing. N.W.: validation and theoretical calculation. M.A.: validation and investigation. L.L.: supervision, project designment, funding acquisition, review, and editing.

Data Availability Statement

The data that support the findings of this study are available in the Supporting Information of this article.

Keywords

hollow nanotubes, interlayer space, Li–S batteries, N-doped ${\rm MoS}_2$, sacrifice template

Received: April 10, 2023 Revised: July 23, 2023 Published online: August 15, 2023

- [1] D. Lu, X. Wang, Y. Hu, L. Yue, Z. Shao, W. Zhou, L. Chen, W. Wang, Y. Li, Adv. Funct. Mater. 2023, 33, 2212689.
- [2] J. Wu, J. Huang, Y. Cui, D. Miao, X. Ke, Y. Lu, D. Wu, Adv. Mater. 2023, 35, 2211471.
- [3] X. Zhang, G. Hu, K. Chen, L. Shen, R. Xiao, P. Tang, C. Yan, H.-M. Cheng, Z. Sun, F. Li, Energy Stor. Mater. 2022, 45, 1144.

16136829, 2023, 48, Downloaded from https://onlinelibrary.wiley.com/doi/10.1002/smll.20203015 by National Taiwan University, Wiley Online Library on [05/122023]. See the Terms and Conditions (https://onlinelibrary.wiley

on Wiley Online Library for rules

of use; OA articles are governed by the applicable Creative Commons

- [4] M. Zhang, L. Wang, B. Wang, B. Zhang, X. Sun, D. Wang, Z. Kong, L. Xu, J. Mater. Chem. 2021, 9, 6538.
- [5] X. Song, D. Tian, Y. Qiu, X. Sun, B. Jiang, C. Zhao, Y. Zhang, L. Fan, N. Zhang, Adv. Funct. Mater. 2021, 32, 2109413.
- [6] A. Fu, C. Wang, F. Pei, J. Cui, X. Fang, N. Zheng, Small 2019, 15, 1804786.
- [7] X. Wei, Y. Luo, X. Du, L. Wu, G. Liu, J. Li, Chem. Eng. J. 2023, 454, 140152
- [8] B. Yan, X. Li, W. Xiao, J. Hu, L. Zhang, X. Yang, J. Mater. Chem. 2020, 8. 17848.
- [9] X. Yang, S. Chen, W. Gong, X. Meng, J. Ma, J. Zhang, L. Zheng, H. D. Abruna, J. Geng, Small 2020, 16, 2004950.
- [10] R. Zhang, Y. Dong, M. A. Al-Tahan, Y. Zhang, R. Wei, Y. Ma, C. Yang, J. Zhang, J. Energy Chem. 2021, 60, 85.
- [11] Y. Cao, Y. Lin, J. Wu, X. Huang, Z. Pei, J. Zhou, G. Wang, Chem-SusChem. 2020, 13, 1392.
- [12] J. Wu, X. Li, H. Zeng, Y. Xue, F. Chen, Z. Xue, Y. Ye, X. Xie, J. Mater. Chem. 2019, 7, 7897.
- [13] Z. Deng, H. Jiang, Y. Hu, Y. Liu, L. Zhang, H. Liu, C. Li, Adv. Mater. 2017. 29. 1603020.
- [14] X. Chen, S. Zeng, H. Muheiyati, Y. Zhai, C. Li, X. Ding, L. Wang, D. Wang, L. Xu, Y. He, Y. Qian, ACS Energy Lett. 2019, 4, 1496.
- [15] Q. Chen, S. Sun, T. Zhai, M. Yang, X. Zhao, H. Xia, Adv. Energy Mater. 2018, 8, 1800054.
- [16] H. Zhang, M. Zou, W. Zhao, Y. Wang, Y. Chen, Y. Wu, L. Dai, A. Cao, ACS Nano. 2019, 13, 3982.
- [17] B. Wang, L. Wang, D. Ding, Y. Zhai, F. Wang, Z. Jing, X. Yang, Y. Kong, Y. Qian, L. Xu, Adv. Mater. 2022, 34, 2204403.
- [18] S. Bolar, S. Shit, N. C. Murmu, P. Samanta, T. Kuila, ACS Appl. Mater. Interfaces 2021, 13, 765.
- [19] H. Lim, S. Yu, W. Choi, S. O. Kim, ACS Nano. 2021, 15, 7409.
- [20] Y. L. Zhong, W. X. Dai, D. Liu, W. Wang, L. T. Wang, J. P. Xie, R. Li, Q. L. Yuan, G. Hong, Small 2021, 17, 2101576.
- [21] Y. Li, M. Chen, H. Liu, P. Zeng, D. Zhang, H. Yu, X. Zhou, C. Guo, Z. Luo, Y. Wang, B. Chang, X. Wang, Chem. Eng. J. 2021, 425.
- [22] J. Cho, S. Ryu, Y. J. Gong, S. Pyo, H. Yun, H. Kim, J. Lee, J. Yoo, Y. S. Kim, Chem. Eng. J. 2022, 439, 135568.
- [23] M. Tebyetekerwa, J. Zhang, K. Liang, T. Duong, G. P. Neupane, L. Zhang, B. Liu, T. N. Truong, R. Basnet, X. Qiao, Z. Yin, Y. Lu, D. Macdonald, H. T. Nguyen, Adv. Mater. 2019, 31, 1900522.
- [24] I. Marriam, M. Tebyetekerwa, H. Chen, H. Chathuranga, N. Motta, J. A. Alarco, Z.-J. He, J.-C. Zheng, A. Du, C. Yan, J. Mater. Chem. 2023, 11, 2670.

- [25] M. Shi, Z. Liu, S. Zhang, S. Liang, Y. Jiang, H. Bai, Z. Jiang, J. Chang, J. Feng, W. Chen, H. Yu, S. Liu, T. Wei, Z. Fan, Adv. Energy Mater. 2022, 12. 2103657.
- [26] Y. Xu, J. Yang, T. Liao, R. Ge, Y. Liu, J. Zhang, Y. Li, M. Zhu, S. Li, W. Li, Chem. Eng. J. 2022, 431, 134126.
- [27] X. Liang, J. Cai, S. Qiu, S. Niu, Y. Liu, X. Wang, G. Wang, Z. Chen, M. Chen, J. Mater. Chem. 2022, 10, 23780.
- [28] Y. You, Y. Ye, M. Wei, W. Sun, Q. Tang, J. Zhang, X. Chen, H. Li, J. Xu, Chem. Eng. J. 2019, 355, 671.
- [29] Y. Liu, M. Han, Q. Xiong, S. Zhang, C. Zhao, W. Gong, G. Wang, H. Zhang, H. Zhao, Adv. Energy Mater. 2019, 9, 1803935.
- [30] Y. Mo, K. Yang, J. Lin, M. Liu, G. Ye, J. Yu, J. Mater. Chem. 2023,, 11, 6349.
- [31] T. Z. Hou, W. T. Xu, X. Chen, H. J. Peng, J. Q. Huang, Q. Zhang, Angew. Chem., Int. Ed. 2017, 56, 8178.
- [32] Y. Yang, W. Wang, L. Li, B. Li, J. Zhang, J. Mater. Chem. 2020, 8, 3692.
- [33] Y. Zhang, X. Ge, Q. Kang, Z. Kong, Y. Wang, L. Zhan, Chem. Eng. J. 2020, 393, 124570.
- [34] B. Liu, S. Huang, D. Kong, J. Hu, H. Y. Yang, J. Mater. Chem. 2019, 7, 7604.
- [35] W. Zhang, D. Hong, Z. Su, S. Yi, L. Tian, B. Niu, Y. Zhang, D. Long, Energy Stor. Mater. 2022, 53, 404.
- [36] Y. Gong, Y. Wang, Z. Fang, S. Zhao, Y.-s. He, W. Zhang, J. Mu, L. Zhang, Z.-F. Ma, Chem. Eng. J. 2022, 446, 136943.
- [37] D. Lei, W. Shang, X. Zhang, Y. Li, S. Qiao, Y. Zhong, X. Deng, X. Shi, Q. Zhang, C. Hao, X. Song, F. Zhang, ACS Nano 2021, 15, 20478.
- [38] P. Guo, W. Chen, Y. Zhou, F. Xie, G. Qian, P. Jiang, D. He, X. Lu, Small **2022**. 18. 2205158.
- [39] J. Zhang, G. Xu, Q. Zhang, X. Li, Y. Yang, L. Yang, J. Huang, G. Zhou, Adv. Sci. 2022, 9, 2201579.
- [40] T. S. Sahu, G. A. V, I. Pal, S. Sau, M. Gautam, B. R. K. Nanda, S. Mitra, Small 2022, 18, 2203222.
- [41] R. Fang, H. Xu, B. Xu, X. Li, Y. Li, J. B. Goodenough, Adv. Funct. Mater.
- **2020**, 31, 2001812.
- [42] J. Cai, Y. Song, X. Chen, Z. Sun, Y. Yi, J. Sun, Q. Zhang, J. Mater. Chem. 2020, 8, 1757.
- [43] C. Dai, L. Hu, X. Li, Q. Xu, R. Wang, H. Liu, H. Chen, S.-J. Bao, Y. Chen, G. Henkelman, C. M. Li, M. Xu, Nano Energy 2018, 53,
- [44] D. Tian, X. Song, Y. Qiu, X. Sun, B. Jiang, C. Zhao, Y. Zhang, X. Xu, L. Fan, N. Zhang, ACS Nano 2021, 15, 16515.
- [45] Z. Shen, Z. Zhang, M. Li, Y. Yuan, Y. Zhao, S. Zhang, C. Zhong, J. Zhu, J. Lu, H. Zhang, ACS Nano 2020, 14, 6673.